

# Dumbbell-like Bifunctional Au–Fe<sub>3</sub>O<sub>4</sub> Nanoparticles

Heng Yu,<sup>†</sup> Min Chen,<sup>†</sup> Philip M. Rice,<sup>‡</sup> Shan X. Wang,<sup>§</sup> R. L. White,<sup>§</sup> and Shouheng Sun<sup>\*,†,‡,§</sup>

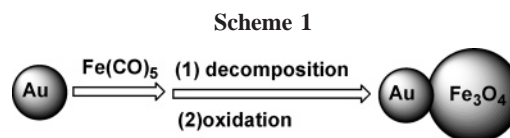
IBM T. J. Watson Research Center, Yorktown Heights, New York 10598, IBM Almaden Research Center, San Jose, California 95120, Department of Materials Science and Engineering and Department of Electrical Engineering, Stanford University, Stanford, California 94305, Department of Chemistry, Brown University, Providence, Rhode Island 02912

Received December 10, 2004; Revised Manuscript Received January 6, 2005

## ABSTRACT

Dumbbell-like Au–Fe<sub>3</sub>O<sub>4</sub> nanoparticles are synthesized using decomposition of Fe(CO)<sub>5</sub> on the surface of the Au nanoparticles followed by oxidation in 1-octadecene solvent. The size of the particles is tuned from 2 to 8 nm for Au and 4 nm to 20 nm for Fe<sub>3</sub>O<sub>4</sub>. The particles show the characteristic surface plasmon absorption of Au and the magnetic properties of Fe<sub>3</sub>O<sub>4</sub> that are affected by the interactions between Au and Fe<sub>3</sub>O<sub>4</sub>. The dumbbell is formed through epitaxial growth of iron oxide on the Au seeds, and the growth can be affected by the polarity of the solvent, as the use of diphenyl ether results in flower-like Au–Fe<sub>3</sub>O<sub>4</sub> nanoparticles.

Nanocomposites containing two or more different nanoscale functionalities are attractive candidates for advanced nanomaterials. With controlled structure and interface interactions, these nanocomposites can exhibit novel physical and chemical properties that will be essential for future technological applications. Core/shell nanostructures<sup>1–3</sup> and exchange-coupled magnetic nanocomposites<sup>4,5</sup> are two well-known composite systems that have shown enhanced optical, magnetic, and catalytic properties compared to their individual single-component materials. Here we report on a general synthesis of dumbbell-like bifunctional composite nanoparticles of Au–Fe<sub>3</sub>O<sub>4</sub> with Au and Fe<sub>3</sub>O<sub>4</sub> in nanometer contact. The size of the particles is tuned from 2 to 8 nm for Au and 4 nm to 20 nm for Fe<sub>3</sub>O<sub>4</sub>. The nanocontact between Au and Fe<sub>3</sub>O<sub>4</sub> results in red-shift of the surface plasmon of the Au and slow increase in magnetization of the small Fe<sub>3</sub>O<sub>4</sub> (8 nm or smaller). The dumbbell structure is formed through epitaxial growth of iron oxide on the Au seeds, and the growth can be affected by the polarity of the solvent, as the use of more polar solvent leads to flower-like Au–Fe<sub>3</sub>O<sub>4</sub> composite particles. The Au–Fe<sub>3</sub>O<sub>4</sub> can be readily converted into Au–Fe<sub>2</sub>O<sub>3</sub> ( $\gamma$ -Fe<sub>2</sub>O<sub>3</sub> or  $\alpha$ -Fe<sub>2</sub>O<sub>3</sub>), making it possible for systematic studies of nanoscale interactions and their effects on physical and chemical properties of the Au–iron oxide nanocomposites.



The bifunctional composite nanostructure containing Au is traditionally obtained by physical deposition of a thin Au film onto a spherical oxide particle,<sup>6–8</sup> adsorption of HAuCl<sub>4</sub> on the TiO<sub>2</sub> surface followed by reduction,<sup>9</sup> or via electroplating through the nanoscale templates.<sup>10,11</sup> A similar structure is also observed from the reaction intermediate in the catalytic growth of Ge nanowires using Au nanoparticles as a catalyst.<sup>12</sup> Recently, solution phase chemical syntheses have been applied to synthesize similarly structured bifunctional nanocomposites, including CdSe–Au from selective growth of Au tips onto CdSe rods/tetrapods.<sup>13–15</sup> The dumbbell-like nanoparticles reported here have several distinct advantages over the previous bifunctional systems: they can be made directly from a solution-phase synthesis without any pretreatment of the particle surface; the structure contains size-tunable Au and Fe<sub>3</sub>O<sub>4</sub> with size of any one kind of particles being controlled up to 20 nm; the Au–Fe<sub>3</sub>O<sub>4</sub> can be further converted to Au–Fe<sub>2</sub>O<sub>3</sub> and Au–Fe, leading to a rich variety of optic, magnetic, and chemical properties.

The dumbbell-like Au–Fe<sub>3</sub>O<sub>4</sub> nanoparticles were prepared via the decomposition of iron pentacarbonyl, Fe(CO)<sub>5</sub>, over the surface of the Au nanoparticles followed by oxidation under air, as illustrated in Scheme 1. The Au nanoparticles

\* Corresponding author. E-mail: ssun@brown.edu.

<sup>†</sup> IBM T. J. Watson Research Center.

<sup>‡</sup> IBM Almaden Research Center.

<sup>§</sup> Stanford University.

<sup>#</sup> Brown University.

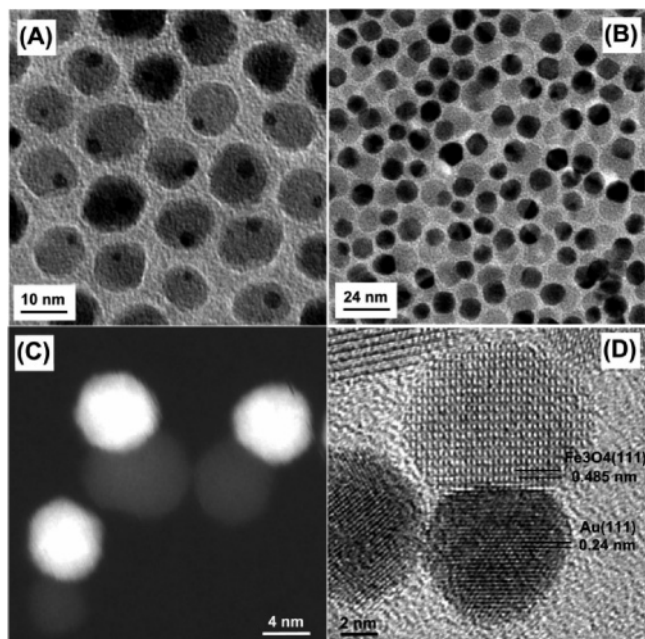


**Figure 1.** TEM and STEM images of the dumbbell-like Au-Fe<sub>3</sub>O<sub>4</sub> nanoparticles: (A) TEM image of the 3–14 nm Au-Fe<sub>3</sub>O<sub>4</sub> particles; (B) TEM image of the 8–14 nm Au-Fe<sub>3</sub>O<sub>4</sub> particles; (C) HAADF-STEM image of the 8–9 nm Au-Fe<sub>3</sub>O<sub>4</sub> particles; and (D) HRTEM image of one 8–12 nm Au-Fe<sub>3</sub>O<sub>4</sub> particle. The specimens for TEM and STEM analyses were prepared by room-temperature deposition of the hexane dispersions of the particles on carbon-coated copper grids. TEM images were acquired using a JEOL 2010F operated at 200 kV. The HAADF-STEM image was acquired by digitally scanning a 3 Å diameter electron beam across a region large enough to include several of the dumbbells. An annular detector set at a camera length so that it collected only electrons scattered beyond approximately 40 mrad and measured the integrated electron count during the 25 microsecond dwell time at each point.

were either synthesized in situ by injecting HAuCl<sub>4</sub> solution into the reaction mixture or pre-made using a modified synthetic procedure.<sup>16</sup> Mixing Au nanoparticles with Fe(CO)<sub>5</sub> in 1-octadecene solvent in the presence of oleic acid and oleylamine and heating the mixture to reflux (~300 °C) followed by room-temperature oxidation under air led to dumbbell-like Au-Fe<sub>3</sub>O<sub>4</sub> nanoparticles.<sup>16</sup> The size of the Au particles was tuned by controlling the temperature at which the HAuCl<sub>4</sub> was injected, or by controlling the HAuCl<sub>4</sub>/oleylamine ratio. For example, injecting HAuCl<sub>4</sub> solution into the reaction mixture containing Fe(CO)<sub>5</sub> at 120 °C led to ~2 nm Au particles, while injection at 160 °C or 180 °C gave 4 or 6 nm Au particles. The size of the Fe<sub>3</sub>O<sub>4</sub> particles was controlled by adjusting the ratio between Fe(CO)<sub>5</sub> and Au. More Fe(CO)<sub>5</sub> led to larger Fe<sub>3</sub>O<sub>4</sub> nanoparticles. We found that Au-Fe<sub>3</sub>O<sub>4</sub> particles with Au up to 8 nm and Fe<sub>3</sub>O<sub>4</sub> up to 20 nm were readily stabilized in hexane.<sup>16</sup>

Figure 1A-B show two transmission electron microscopy (TEM) images of the dumbbell-like Au-Fe<sub>3</sub>O<sub>4</sub> nanoparticles with Fe<sub>3</sub>O<sub>4</sub> at around 14 nm and Au at 3 and 8 nm, respectively. Statistical analyses on the size of the various dumbbell particles show the standard deviation for the diameter of Au is within 15% and that of Fe<sub>3</sub>O<sub>4</sub> within 12%. The Au particles appear black and Fe<sub>3</sub>O<sub>4</sub> are light colored

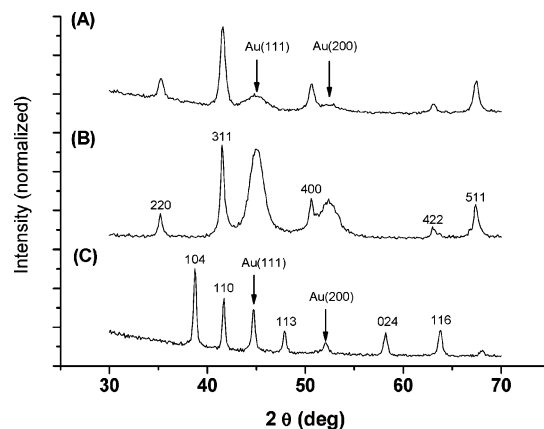


**Figure 2.** X-ray diffraction patterns of Au-Fe<sub>3</sub>O<sub>4</sub> nanoparticles with representative index on typical peaks: (A) 3–14 nm Au-Fe<sub>3</sub>O<sub>4</sub>, (B) 8–14 nm Au-Fe<sub>3</sub>O<sub>4</sub>, and (C) Au-α-Fe<sub>2</sub>O<sub>3</sub> after oxidative annealing of the sample from (B). The samples were deposited from their hexane dispersions on Si (100) substrates and dried under ambient conditions. The diffraction patterns were collected on a Siemens D-500 diffractometer under Co Kα radiation ( $\lambda = 1.788965$  Å).

in the image because Au has a higher electron density and allows fewer electrons to transmit. Figure 1C is the high angle annular dark field scanning transmission electron microscopy (HAADF-STEM) image of several dumbbell nanoparticles. The brightness in the image reflects the intensity of scattered electrons from different substance and is proportional to the atomic number (*Z*).<sup>17</sup> In Figure 1C, the Au particles, which have the higher *Z* compared to the Fe<sub>3</sub>O<sub>4</sub> particles, are imaged as brighter dots.

Figure 1D is a typical high-resolution TEM (HRTEM) image of a dumbbell particle with Fe<sub>3</sub>O<sub>4</sub> at 12 nm and Au at 8 nm. The lattice fringes in each of the particles correspond to atomic planes within the particle, indicating that both particles are single crystals. The distance between two adjacent planes in Fe<sub>3</sub>O<sub>4</sub> is measured to be 0.485 nm, corresponding to (111) planes in the inverse spinel structured Fe<sub>3</sub>O<sub>4</sub> and that in Au is 0.24 nm, resulting from a group of (111) planes in fcc structured Au. The crystalline nature of the dumbbell particles can also be characterized by X-ray diffraction (XRD). Figure 2 shows representative XRD patterns of the Au-Fe<sub>3</sub>O<sub>4</sub> nanoparticles with Fe<sub>3</sub>O<sub>4</sub> at around 14 nm and Au around 3 nm (Figure 2A) and 8 nm (Figure 2B), respectively. The position and relative intensity of all diffraction peaks match with standard Fe<sub>3</sub>O<sub>4</sub> and Au powder diffraction data, indicating that the synthesis yields single crystalline inverse spinel structured Fe<sub>3</sub>O<sub>4</sub> and fcc structured Au. The Fe<sub>3</sub>O<sub>4</sub> structure is further characterized by its chemical transformation under thermal annealing condition. After annealing at 500 °C under Ar for 1 h, the particles show the same XRD pattern as in Figure 2A, indicating no structure change. This is consistent with the structural stability observed in Fe<sub>3</sub>O<sub>4</sub> nanoparticles at high temperatures.<sup>18</sup> However, if the particles were annealed at 300 °C under oxygen for 3 h first, then under Ar at 500 °C for 1 h, their XRD showed two sets of different peaks with one being fcc Au and the other related to α-Fe<sub>2</sub>O<sub>3</sub> (Figure 2C). It is known that Fe<sub>3</sub>O<sub>4</sub> nanoparticles can be oxidized to γ-Fe<sub>2</sub>O<sub>3</sub>

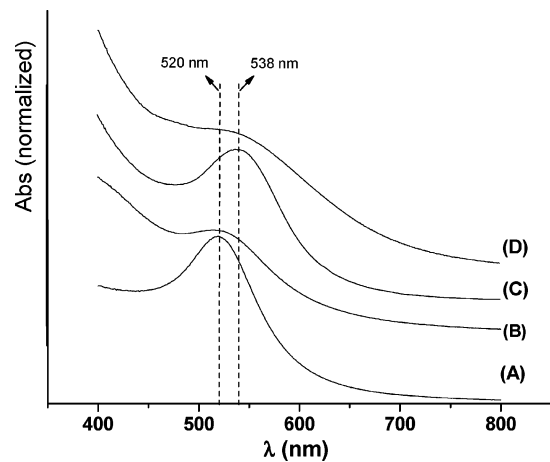


**Figure 3.** UV-vis spectra of the Au and Au-Fe<sub>3</sub>O<sub>4</sub> nanoparticles: (A) 8 nm Au; (B) 4 nm Au; (C) 7–14 nm Au-Fe<sub>3</sub>O<sub>4</sub>; and (D) 3–14 nm Au-Fe<sub>3</sub>O<sub>4</sub>. The spectra were collected on a Lambda 9 UV/VIS/NIR spectrometer in the wavelength from 350 to 800 nm. All particles were dispersed in hexane.

that is thermally unstable and can be converted into  $\alpha$ -Fe<sub>2</sub>O<sub>3</sub> particles at temperatures above 450 °C.<sup>18</sup> The chemical transformation observed from Figure 2B to Figure 2C indicates that Fe<sub>3</sub>O<sub>4</sub> is indeed formed in the dumbbell structure and can be converted to  $\gamma$ -Fe<sub>2</sub>O<sub>3</sub> and further to  $\alpha$ -Fe<sub>2</sub>O<sub>3</sub> under the high-temperature annealing conditions.

The dumbbell-like Au-Fe<sub>3</sub>O<sub>4</sub> composite nanoparticles show red-shift of the surface plasmon of the Au due to its nanocontact with Fe<sub>3</sub>O<sub>4</sub>. It is known that for Au particles with sizes ranging from 5 to 20 nm in diameter, the electrons are trapped in the small Au metal box and show a characteristic collective oscillation frequency of the plasmon resonance, giving rise to the plasmon resonance band at around 520 nm.<sup>19</sup> The exact absorption position varies with particle morphology and particle surface coating. Figure 3 is the UV-vis spectra of the Au and Au-Fe<sub>3</sub>O<sub>4</sub> particles prepared in this work and dispersed in hexane. The peaks at 520 nm for Au nanoparticles is independent of the size and concentration of the particles but the width was found to increase with decreased size of the Au particles (Figure 3A,B), consistent with the observation from the Au nanoparticles made by different methods.<sup>19</sup> However, once attached to Fe<sub>3</sub>O<sub>4</sub>, the Au particles show plasmon absorption at 538 nm (Figure 3C&D), a  $\sim$ 18 nm red-shift from that of the pure Au particles. This could result from the charge variation of the Au particles within the dumbbell structure. Previous studies show that excess electrons on the Au particles can cause the plasmon absorption shift to shorter wavelength; whereas electron deficiency will shift the absorption to longer wavelength.<sup>19</sup> The red shift of the surface plasmon spectra of the dumbbell structure indicates that the interface communication between Au and Fe<sub>3</sub>O<sub>4</sub> results in deficient electron population on Au.

The interface communication between the nanoscale Au and Fe<sub>3</sub>O<sub>4</sub> also leads to the change of magnetization behaviors of the Fe<sub>3</sub>O<sub>4</sub> nanoparticles, especially for those smaller than 8 nm. Figure 4 shows the hysteresis loops measured at room temperature for Au-Fe<sub>3</sub>O<sub>4</sub> particles with

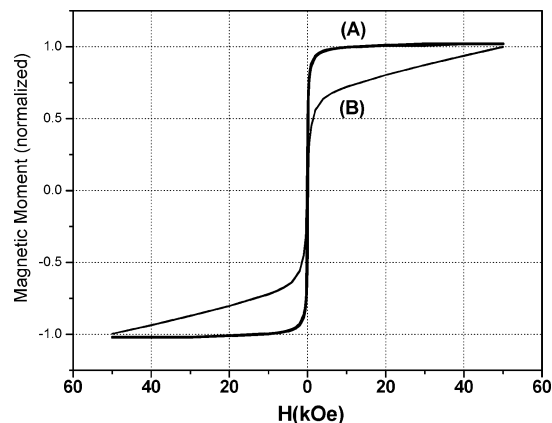


**Figure 4.** Hysteresis loops of the Au-Fe<sub>3</sub>O<sub>4</sub> particles measured at room temperature: (A) 3–14 nm Au-Fe<sub>3</sub>O<sub>4</sub> and (B) 3–6 nm Au-Fe<sub>3</sub>O<sub>4</sub> particles. The particles were deposited on Si (100) substrates from their hexane dispersions and dried under ambient conditions. The measurements were carried out using a MPMS2 Quantum Design SQUID magnetometer with fields up to 5 T.

Au being 3 nm and Fe<sub>3</sub>O<sub>4</sub> 14 nm (Figure 4A) and 6 nm (Figure 4B), respectively. Like Fe<sub>3</sub>O<sub>4</sub> nanoparticles, the dumbbell particles are superparamagnetic at room temperature. The 3–14 nm dumbbell particles show loops similar to the 14 nm Fe<sub>3</sub>O<sub>4</sub> nanoparticles with saturation moment reaching 80 emu/g (Figure 4A), a value that is close to the related Fe<sub>3</sub>O<sub>4</sub> nanoparticles due to the negligible weight percentage of 3 nm Au in the composite. The 3–6 nm dumbbell particles, however, show a loop of slow increase in moment with the field up to 5 T (Figure 4B). This may be caused by both thermal agitation and the surface spin canting of the small particles.<sup>20</sup>

The Au-Fe<sub>3</sub>O<sub>4</sub> structure is likely derived from the epitaxial growth of Fe<sub>3</sub>O<sub>4</sub> on the Au seeds as Au has an fcc structure with  $a = 4.08 \text{ \AA}$ , while Fe<sub>3</sub>O<sub>4</sub> has a cubic structure with  $a = 8.35 \text{ \AA}$ , which is within 3% of being exactly double. Once the Fe<sub>3</sub>O<sub>4</sub> starts to nucleate on an Au, the free electrons from the Au must compensate for the charge induced by the polarized plane at the interface. As the Au particle has only a very limited source of electrons, this compensation makes all other facets of the Au nanoparticle electron deficient and unsuitable for multi-nucleation, giving only the dumbbell structure. If the polarity of the solvent used for the synthesis is increased, the Au nanoparticles could compensate for the apparent electron density loss with charges from the solvent, allowing nucleation on multiple facets. Experimentally, we did synthesize the flower-like Au-Fe<sub>3</sub>O<sub>4</sub> nanoparticles by switching the solvent from nonpolar hydrocarbon to slightly polarized diphenyl ether.<sup>16</sup> Figure 5 shows the TEM images of such flower-like nanoparticles with the faceted Au core being  $\sim$ 8 nm and radial length of the Fe<sub>3</sub>O<sub>4</sub> at  $\sim$ 4 nm, indicating clearly the multi-nucleation of iron oxide on the faceted Au seeds.

The present report demonstrates a simple chemical synthesis of dumbbell-like Au-Fe<sub>3</sub>O<sub>4</sub> nanoparticles with the Au and the Fe<sub>3</sub>O<sub>4</sub> being in nanometer contact. The size, structure and chemical nature of each part of the dumbbell are controlled by regulating the synthetic conditions. The dumb-

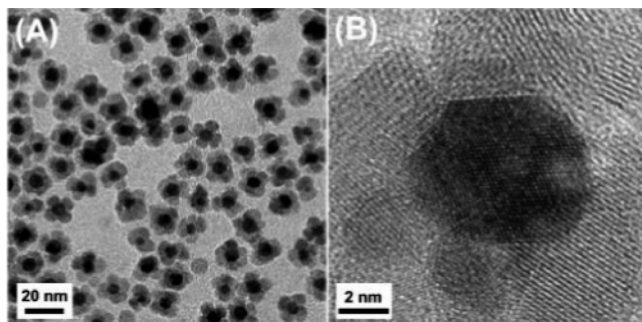


**Figure 5.** (A) Low resolution TEM and (B) HRTEM images of flower-like Au–Fe<sub>3</sub>O<sub>4</sub> nanoparticles.

bell structure offers the particles with two distinct surfaces and functionalities. With Au, one can use the well-developed gold–thiol chemistry for site-specific assembly and attachment of thiol-terminated molecules, especially biomolecules;<sup>21–23</sup> with Fe<sub>3</sub>O<sub>4</sub>, one can apply a highly sensitive magnetic sensor to detect the magnetic signal of the particles.<sup>24</sup> The electron deficient Au in the dumbbell structure has similar configuration to the Au catalyst on metal oxide surface<sup>25</sup> and may be an efficient catalyst for CO oxidation. With the control of functionalities and the interface interactions, these dumbbell structures should become ideal model systems for studying structural and interface effects on physical and chemical properties, and may evolve as useful nanoscale building blocks for nanoelectronic, biological, and catalytic applications.

**Acknowledgment.** The work was supported in part by DARPA through ONR under grant Nos. N00014-01-1-0885. M.C. thanks DARPA for support under grant Nos. DAAD 19-03-1-0038 through the University of Texas, Arlington.

**Supporting Information Available:** Synthesis of Au nanoparticles and Au–Fe<sub>3</sub>O<sub>4</sub> composite nanoparticles. This

material is available free of charge via the Internet at <http://pubs.acs.org>.

## References

- (1) Peng, X.; Schlamp, M. C.; Kadavanich, A. V.; Alivisatos, A. P. *J. Am. Chem. Soc.* **1997**, *119*, 7019.
- (2) Malik, M. A.; O'Brien, P.; Revaprasadu, N. *Chem. Mater.* **2002**, *14*, 2004.
- (3) Decker, S.; Klabunde, K. J. *J. Am. Chem. Soc.* **1996**, *118*, 12465.
- (4) Zeng, H.; Li, J.; Liu, J. P.; Wang, Z. L.; Sun, S. *Nature* **2002**, *420*, 395.
- (5) Zeng, H.; Li, J.; Wang, Z. L.; Liu, J. P.; Sun, S. *Nano Lett.* **2004**, *4*, 187.
- (6) Bao, Z.; Chen, L.; Weldon, M.; Chandross, E.; Cherniavskaya, O.; Dai, Y.; Tok, J. B.-H. *Chem Mater.* **2002**, *14*, 24.
- (7) Lu, Y.; Xiong, H.; Jiang, X.; Xia, Y.; Prentiss, M.; Whitesides, G. M. *J. Am. Chem. Soc.* **2003**, *125*, 12724.
- (8) Behrend, C. J.; Anker, J. N.; McNaughton, B. H.; Brasuel, M.; Philbert, M. A.; Kopelman, R. *J. Phys. Chem. B* **2004**, *108*, 10408.
- (9) Dawson, A.; Kamat, P. V. *J. Phys. Chem. B* **2001**, *106*, 960.
- (10) Reich, D. H.; Tanase, M.; Hultgren, A.; Bauer, L. A.; Chen, C. S.; Meyer, G. J. *J. Appl. Phys.* **2003**, *93*, 7275.
- (11) Charnay, C.; Lee, A.; Man, S.-Q.; Moran, C. E.; Radloff, C.; Bradley, R. K.; Halas, N. J. *J. Phys. Chem. B* **2003**, *107*, 7327.
- (12) Wu, Y.; Yang, P. *J. Am. Chem. Soc.* **2001**, *123*, 3165.
- (13) Kokari, T.; Rothenberg, E.; Popov, I.; Costi, R.; Banin, U. *Science* **2004**, *304*, 1787.
- (14) Gu, H.; Zheng, R.; Zhang, X.; Xu, B. *J. Am. Chem. Soc.* **2004**, *126*, 5664.
- (15) Teranishi, T.; Inoue, Y.; Nakaya, M.; Oumi, Y.; Sano, T. *J. Am. Chem. Soc.* **2004**, *126*, 9914.
- (16) See the Supporting Information.
- (17) Nellist, D.; Pennycook, S. J. *Ultramicroscopy* **1999**, *78*, 111.
- (18) Sun, S.; Zeng, H.; Robinson, D. B.; Raoux, S.; Rice, P. M.; Wang, S. X.; Li, G. *J. Am. Chem. Soc.* **2004**, *126*, 273.
- (19) Daniel, M.-C.; Astruc, D. *Chem. Rev.* **2004**, *104*, 293.
- (20) Martinez, B.; Obradors, X.; Balcells, L.; Rouanet, A.; Monty, C. *Phys. Rev. Lett.* **1998**, *80*, 181.
- (21) Loweth, C. J.; Brett Caldwell, W.; Peng, X.; Alivisatos, A. P.; Schultz, P. G. *Angew. Chem., Int. Ed.* **1999**, *38*, 1808.
- (22) Storhoff, J. J.; Lazarides, A. A.; Mirkin, C. A.; Letsinger, R. L.; Mucic, R. C.; Schatz, G. C. *J. Am. Chem. Soc.* **2000**, *122*, 4640.
- (23) Cao, Y. C.; Jin, R.; Mirkin, C. A. *Science* **2002**, *297*, 1536.
- (24) Li, G.; Wang, S.; Sun, S. *IEEE Trans. Magn.* **2004**, *40*, 3000.
- (25) Haruta, M.; Kobayashi, T.; Sano, H.; Yamada, N. *Chem. Lett.* **1987**, 405.

NL047955Q